Math. Model. Nat. Phenom. 20 (2025) 6
https://doi.org/10.1051/mmnp/2025010

Mathematical Modelling of Natural Phenomena
www.mmnp-journal.org

ON NANOWIRE MORPHOLOGICAL INSTABILITY AND PINCH-OFF BY SURFACE ELECTROMIGRATION

Mikhail Khenner[1,2,*]

Abstract. Surface diffusion and surface electromigration may lead to a morphological instability of thin solid films and nanowires. In this paper two nonlinear analyses of a morphological instability are developed for a single-crystal cylindrical nanowire that is subjected to an axial current. These treatments extend the conventional linear stability analyses without surface electromigration, that manifest a Rayleigh–Plateau instability. A weakly nonlinear analysis is done slightly above the Rayleigh–Plateau (longwave) instability threshold. It results in a one-dimensional Sivashinsky amplitude equation that describes a blow-up of a surface perturbation amplitude in a finite time. This is a signature of a pinching singularity of a cylinder radius, which leads to a wire separation into a disjoint segments. The time- and electric field-dependent dimensions of the focusing self-similar amplitude profile approaching a blow-up are characterized via the scaling analysis. Also, a weakly nonlinear multi-scale analysis is done at the arbitrary distance above a longwave or a shortwave instability threshold. The time- and electric field-dependent Fourier amplitudes of the major instability modes are derived and characterized.

Mathematics Subject Classification. 74-10, 74F05, 74H15, 74H35, 74H55, 35Q74, 35Q79.

Received November 11, 2024. Accepted February 20, 2025.

1. Introduction

Surface electromigration [1–3] is a well-known and efficient method to guide morphological changes of thin films by surface diffusion. In particular, it has been used to manufacture nanocontacts by breaking of thin films and nanowires via a controlled pinch-offs [4–6]. Such nanocontacts are required for engineering and biomedical applications, for example, for measurement of the electrical conductance and electronic properties of a molecule, but forming a quality nanocontact is still a major challenge [7]. To overcome that challenge, the first step should be a basic understanding of a surface electromigration-driven morphological instability of a single-crystal wire that leads to a pinch-off event.

Modeling morphological instabilities of nanowires by a classical approach of accounting for surface diffusion via an evolution partial differential equation (PDE) for a shape variable [8–10] flourished in the 1990s and early 2000s [11–17]. A recent paper emphasizing this approach is by Wang *et al.* [18]. These authors considered a surface area minimization problem, computed a wire pinch-off using a phase-field method, and extended the Rayleigh–Plateau stability condition to finite amplitude perturbations. Also limited Monte Carlo computations

Keywords and phrases: Nanowires, morphological stability, electromigration, singular solutions of PDEs, weakly nonlinear analysis, scaling analysis, multi-scale analysis.

[1] Department of Mathematics, Western Kentucky University, Bowling Green, KY 42101, USA.
[2] Applied Physics Institute, Western Kentucky University, Bowling Green, KY 42101, USA.

* Corresponding author: mikhail.khenner@wku.edu

were published [19]. For predictive applied modeling of a nanocontact fabrication process a multi-physics framework is needed, that explicitly includes a model and a computation of a nanowire pinch-off instability, whereby the latter is triggered and enhanced by the surface current. Since the cited works do not consider the key mass transport mechanism, namely surface electromigration (shortened to electromigration in the rest of the paper), they cannot form a basis for that framework.

Toward the stated goal, in reference [20] this author introduced a PDE-based model for electromigrated cylindrical nanowire deposited on a substrate. That model is complicated by the presence of the contact lines and a non-axisymmetric surface instability modes. A linear stability analysis (LSA) of that model is performed in reference [20], from which a simpler case of axisymmetrically evolving free-standing wire is easily recovered. Axisymmetric modes dominate evolution of surface perturbations for a free-standing wire in the absence of electromigration, *i.e.* when only a natural high-temperature surface diffusion is operative [11]. Provided the axial current and a corresponding diffusion anisotropy that is a function of the axial variable, this is expected to hold when the electromigration is also operative. reference [21] reports a computation of a wire breakup into a chain set of particles for the simpler case. The breakup time and the number of particles that emerge upon a breakup are characterized as a function of the initial surface roughness.

In this communication, also assuming axisymmetrically evolving, free-standing long wire, in Section 4 I perform a weakly nonlinear analysis slightly above the longwave instability threshold. The latter means that a critical (a most dangerous, *i.e.* a fastest growing) sinusoidal perturbation of a uniform surface profile $r(y) = const.$ (where r is a wire radius and y the axial coordinate) has a tiny axial wavenumber $k \to 0$. I derive an amplitude equation via the expansion of a governing PDE up to the terms that are quadratic in the amplitude, whereas LSA is based on the expansion up to linear terms, *i.e.* a linearization procedure. In other words, the perturbation amplitude is finite in the weakly nonlinear analysis. This key underlying assumption is the same in this paper and in Ref. [18]. A finite amplitude is quite likely to occur in experiment [22]. A scaling analysis and a computation of the amplitude equation show that the amplitude becomes unbounded (blows up) in finite time. Following reference [23] and to simplify writing, I will refer to the amplitude approaching a blow-up singularity as a spike. From the analysis I obtain the much needed information on the time-and-electric field-dependent dimensions of the spike. Note that the blow-up singularity of the amplitude (a spike formation) is the signature of a finite-time pinching singularity of a wire radius ($r \to 0$). The (finite) time of a singularity formation is the same for the amplitude singularity and for the radius singularity. In a basic experiment demonstrating a Rayleigh–Plateau instability without electromigration a wire pinches off at multiple locations along the axis, thus several shorter cylindrical wire segments are formed [24, 25]. The spacing between pinch-offs is approximately equal to the most dangerous wavelength. Depending on a new segment's length (that is, depending on whether a Rayleigh–Plateau instability is again operational) a segment may further pinch-off resulting in even shorter segments, or, provided sufficient time, it may transform by surface diffusion into a spherical nanoparticle.

Independent of the weakly nonlinear analysis, in Section 5 I start with the assumption of the initial unstable surface perturbation having an arbitrary finite wavenumber $0 < k < k_c$, where k_c is the instability cut-off wavenumber from LSA, and ask which unstable surface modes are the fastest growing. In this weakly nonlinear multi-scale treatment the spike formation is not considered. (As in the "standard" weakly nonlinear analysis in Section 4, the governing PDE for the surface variable will be expanded to second order in a small parameter that has a meaning of a perturbation amplitude. This explains why I use the term "weakly nonlinear multi-scale analysis".) Nonlinearity of the governing PDE forces a fast distortion of the initial sinusoidal surface perturbation into a general smooth surface shape, and as was just explained, I am interested in finding the fastest growing Fourier modes in its spectrum.

2. The model

Assuming an axisymmetric evolution of a wire surface and a constant electric field E_0 in the axial direction, I consider surface electromigration on a free-standing cylindrical nanowire of radius R_0, see Figure 1. A wire material is fcc metal such as gold. In axisymmetric case the linear stability results in Section 3 also hold for a wire grown laterally on a substrate – if the base state is semi-cylindrical, meaning that a wire surface makes

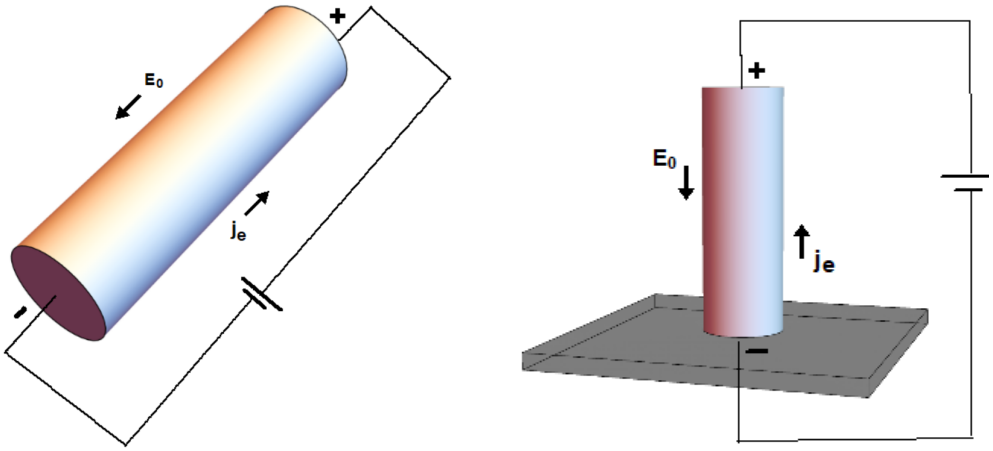

FIGURE 1. Two situations for a free-standing unperturbed cylindrical nanowire (the base state). Left: a nanowire suspended in 3D space, say, by hanging it on a thread attached to a support. Right: a nanowire grown vertically on a horizontal substrate. j_e is the surface electric current that drives the surface electromigration of adatoms via the "electron wind" [1–3].

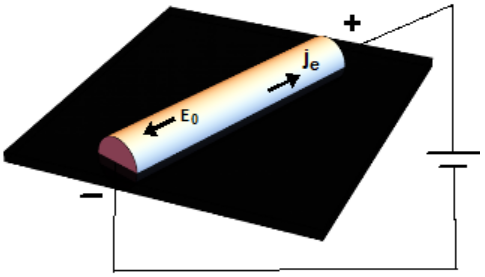

FIGURE 2. Unperturbed cylindrical nanowire grown laterally on a substrate with a 90° contact angle.

a 90° contact angle with the substrate [20] (Fig. 2). This is because when a perturbation is axisymmetric and the contact angle is 90°, a wire does not "feel" the contact lines in the linear approximation. Thus the results of a nonlinear analyses in Sections 4 and 5 for a free-standing wire may be considered as approximations in the case of a laterally grown wire with a 90° contact angle.

Let R_0 and $R_0^4 kT/(D\gamma\Omega^2\nu)$ be the length and the time scales. Here, kT is the thermal energy, γ the surface energy, Ω the atomic volume, and D, ν the surface diffusivity and the surface density of the adatoms. Then the dimensionless wire radius $r(t, y)$ is governed by a nonlinear evolution PDE [20, 21]:

$$r_t = \frac{1}{r}\frac{\partial}{\partial y}\left[M(r_y)\frac{rK_y + E}{\sqrt{1 + r_y^2}}\right], \tag{2.1}$$

where y is the axial variable,

$$K = \frac{1}{r\sqrt{1 + r_y^2}} - \frac{r_{yy}}{\left(1 + r_y^2\right)^{3/2}} \tag{2.2}$$

the mean curvature of the surface, and

$$M(r_y) = \frac{1 + S\cos^2\left[m\left(\arctan r_y + \psi\right)\right]}{1+S} \tag{2.3}$$

the anisotropic diffusional mobility of the adsorbed atoms (adatoms) [26]. Here $S > 0$ is the anisotropy strength, m the number of symmetry axes, and ψ the misorientation angle, *i.e.* this is the angle, in the yz plane, formed by a wire axis and the average orientation of the unit normal to the surface. To reduce the number of parameters in this study it is assumed that a wire axis is along [110] crystalline direction, thus $m = 1$ and $0 \le \psi \le \pi/2$ [27]. Also $E = Q\Delta V R_0^2/(\Omega\gamma\ell)$ is the electric field parameter, where $Q > 0$ is the effective charge of ionized adatoms, ΔV a voltage difference between the front and back faces of a wire, ℓ the wire length, Ω the atomic volume, and γ the surface energy. Note that $E_0 = \Delta V/\ell$, and thus a positivity (a negativity) of E_0 and E depends on the sign of ΔV. When surface diffusion is isotropic ($S = 0 \to M(r_y) = 1$) and the electric field is off ($E = 0$), equation (2.1) reduces to a well-known evolution equation $r_t = \frac{1}{r}\frac{\partial}{\partial y}\left[\frac{rK_y}{\left(1+r_y^2\right)^{1/2}}\right]$ [11, 12], which expresses only the adatom surface diffusion via a surface Laplacian of mean curvature.

The key simplifying physical assumption underlying the above mathematical model is that a current crowding at the tip of a spike is neglected. In the first approximation, a current crowding may be accounted for by replacing E with E/r in equation (2.1) [26, 28, 29]. This change would result in a complex-valued perturbation growth rate in the linear stability analysis in Section 3, with the real part of the growth rate unaffected. Thus an initial surface perturbation would not only grow, but it would also drift along a wire, and thus a pinch-off would occur at a location that is different from the location of a minimum of an initial perturbation. More important is that neglecting a current crowding means neglecting Joule heat production in a wire, which leads to a slower time to a pinch-off – since a higher temperature speeds up the surface diffusion. A wire may even melt before it pinched off [7, 30, 31]. Faceting of a wire surface may also occur [32] and may affect a pinch-off. Lastly, a polycrystal wires are less stable than a single crystal ones due to grain-boundary grooving, which may be enhanced by electromigration. It was shown that the spacing between the wire segments and the size of the segments are smaller for polycrystal wires [33].

3. Linear stability analysis

Equation (2.1) has the trivial solution $r = 1$ (the base state), corresponding to unperturbed cylinder. Introducing a tiny perturbation of the base state, $r = 1 + \xi_0 \mathrm{e}^{\sigma t}\cos ky$, $\xi_0 \ll 1$, and linearizing in ξ_0 gives the growth rate σ and the instability cut-off wavenumber k_c [20]:

$$\sigma(k;E) = \frac{2 + S(1+\cos 2\psi)}{2(1+S)}k^2\left(1-k^2\right) + E\frac{S\sin 2\psi}{1+S}k^2 \equiv \frac{\alpha_1+\alpha_3}{2\left(\alpha_3-1\right)}k^2\left(1-k^2\right) + \frac{\alpha_2}{\alpha_3-1}Ek^2, \tag{3.1}$$

$$k_c(E) = \sqrt{1 + \frac{2SE\sin 2\psi}{2 + S(1+\cos 2\psi)}} \equiv \sqrt{1 + \frac{2\alpha_2 E}{\alpha_1+\alpha_3}}. \tag{3.2}$$

Perturbations with a wavenumbers $0 < k < k_c(E)$ destabilize the base state, since for these wavenumbers $\sigma(k;E) > 0$. This is a longwave instability. Here I introduced a non-negative parameters $\alpha_1 = S\cos 2\psi, \alpha_2 = S\sin 2\psi$ and a positive parameter $\alpha_3 = 2 + S$. At $S = 0$ (isotropy) with either $E = 0$, or $E \neq 0$, equations (3.1) and (3.2) reduce to $\sigma(k;0) = k^2(1-k^2)$ and $k_c(0) = 1$, respectively, which characterize a classical Rayleigh–Plateau instability of a free-standing solid wire [8]. In dimensional coordinates this implies that an axisymmetric sinusoidal perturbation induces instability if and only if its wavelength is longer than the circumference of the undisturbed cylinder.

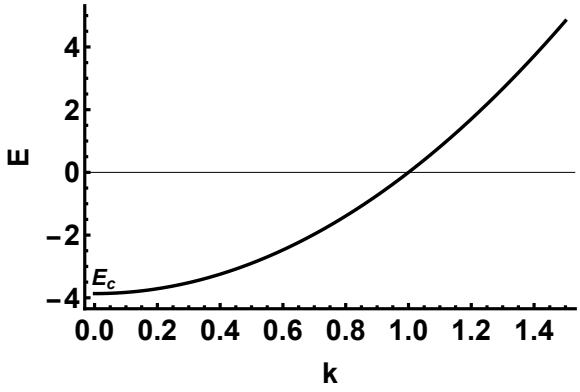

FIGURE 3. The neutral stability curve $E(k)$.

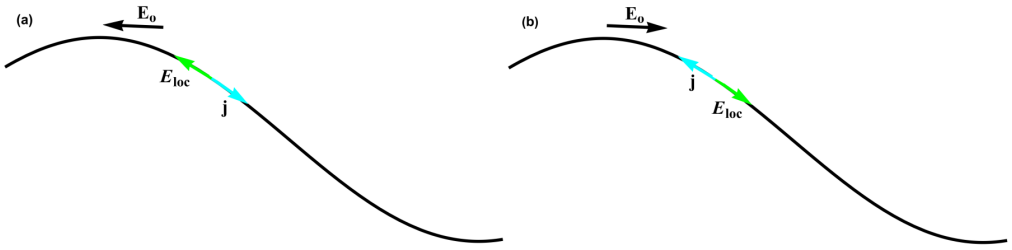

FIGURE 4. (a,b) Sketch of a cross-section of a bump on a wire surface by a plane that is parallel to a wire axis. A projection of a constant electric field E_0 onto a surface, E_{loc}, drives the electromigration adatom flux j in the opposite direction, *i.e.* in the direction of the electron flow j_e. This contributes to either (a) a bump smoothing (stabilization), or to (b) a bump growth (destabilization).

Setting $\sigma = 0$ results in the neutral stability curve $E(k) = \frac{\alpha_1+\alpha_3}{2\alpha_2}\left(k^2 - 1\right)$. Figure 3 shows this curve for $S = 1$ and $\psi = \pi/12$ [20] (these values are fixed for the remainder of this paper). The threshold of a longwave instability is $(k, E_c) = (0, \frac{-(\alpha_1+\alpha_3)}{2\alpha_2}) = (0, -3.866)$. Above the neutral stability curve, *i.e.* for $E > E_c$ the wire is unstable; below the neutral stability curve it is stable. For $E > 0$ the instability is due to a combined action of two destabilizing factors, the electromigration and a surface diffusion. For $E < E_c$ the wire is completely stabilized by electromigration. For $E_c < E < 0$ the stabilizing action of electromigration is weak and the instability due to surface diffusion still emerges. Figure 4 shows why not only the strength of the electric field, but also its direction (determined by a sign of ΔV) matters for a morphological instability. For a gold wire, values of the physical parameters can be taken as: $R_0 = 25$ nm, $\ell = 1000$ nm, $Q = 20|e|$ (here e is the electron charge), $\gamma = 1500$ erg/cm^2, $\Omega = 10^{-22}$ cm^3. Then at $|E_c| = 3.866$ one obtains 0.01 V for the critical value of the applied voltage.

Remark. In reference [18], where electromigration is not considered, a correction to $k_c(0)$ is derived that accounts for the finite perturbation amplitude, *i.e.* the starting assumption $\xi_0 \ll 1$ is replaced by $0 < \xi_0 < 1$. The corrected expression reads $k_c(0) = \sqrt{1 + \xi_0^2}$. For the analyses that follow in Sections 4 and 5 it is not necessary to likewise correct k_c in equation (3.2), since in Section 4 $k \to 0$ (is tiny) and k_c is irrelevant, and in Section 5 k_c is not needed explicitly.

4. Weakly nonlinear analysis slightly above the instability threshold $(k, E) = (0, E_c)$

4.1. Derivation of the amplitude equation for the perturbation of the uniform base state $r = 1$

I start by substituting $r = 1 + \delta\xi(t, y),\ \delta \ll 1$ in the right-hand side of equation (2.1), expanding to second order in δ, and formally adding the coefficients of δ and δ^2. This results in:

$$(\alpha_3 - 1)\,\xi_t = -\left(E\alpha_2 + \frac{1}{2}(\alpha_1 + \alpha_3)\right)\xi_{yy} - \frac{1}{2}(\alpha_1 + \alpha_3)\xi_{yyyy} + \frac{1}{2}(\alpha_1 + \alpha_3)\xi_y^2 - \frac{1}{2}(\alpha_1 + \alpha_3)\xi_{yy}^2$$
$$-(\alpha_1 + \alpha_3)\xi_y\xi_{yyy} + \left[(E\alpha_2 + \alpha_1 + \alpha_3)\xi + \left(2\alpha_2 - \frac{1}{2}E(5\alpha_1 + \alpha_3)\right)\xi_y + \alpha_2\xi_{yyy}\right]\xi_{yy} + \alpha_2\xi_y\xi_{yyyy}. \tag{4.1}$$

LSA results (3.1), (3.2) may be recovered from equation (4.1).

Let $E = E_c + \epsilon E_1, E_1 = \mathcal{O}(1) > 0$. Note that the coefficient of ξ_{yy} changes its sign at $E = E_c$, hence it is proportional to $E - E_c = \epsilon E_1$, which is $\mathcal{O}(\epsilon)$. The balance of the largest nonlinear term $\sim \xi_y^2$ with the linear term $\sim \epsilon\xi_{yy}$ is for $\xi(t, y) = \epsilon\phi(t, y), \phi = \mathcal{O}(1)$. Also, since the linear instability interval is $0 < k < k_c$, where $k_c = \sqrt{1 + \frac{2\alpha_2 E}{\alpha_1+\alpha_3}} = \sqrt{1 - \frac{E}{E_c}} = \sqrt{\frac{-E_1}{E_c}\epsilon} = \mathcal{O}\left(\epsilon^{1/2}\right)$, the appropriate rescaling of the axial coordinate y is $Y = \epsilon^{1/2}y$.

Thus also let:

$$\xi = \epsilon\phi; \quad T = \epsilon^2 t \Leftrightarrow \partial_t = \epsilon^2\partial_T, \quad Y = \epsilon^{1/2}y \Leftrightarrow \partial_y = \epsilon^{1/2}\partial_Y, \tag{4.2}$$

where T, Y are a slow time and a stretched axial variable.

Inserting $E = E_c + \epsilon E_1$ and expansions (4.2) in equation (4.1) I get:

$$\phi_T\epsilon^3 = -\left\{\alpha_2 E_c + \frac{1}{2}(\alpha_1 + \alpha_3)\right\}\phi_{YY}\epsilon^2 + \left\{-a\phi_{YY} - b\left[\phi_{YYYY} - \phi_Y^2 - \phi\phi_{YY}\right]\right\}\epsilon^3 + \mathcal{O}\left(\epsilon^{7/2}\right), \tag{4.3}$$

where $a = \frac{\alpha_2 E_1}{\alpha_3 - 1} = \frac{SE_1 \sin 2\psi}{1+S} = E_1/4 > 0$, $b = \frac{\alpha_1+\alpha_3}{2(\alpha_3-1)} = \frac{2+S(1+\cos 2\psi)}{2(1+S)} \approx 0.966$. Noticing that the coefficient of $\phi_{YY}\epsilon^2$ is zero, in the lowest order ϵ^3 I finally obtain the amplitude equation

$$\phi_T = -a\,\phi_{YY} - b\left[\phi_{YYYY} - \phi_Y^2 - \phi\phi_{YY}\right]. \tag{4.4}$$

Equation (4.4) can be also written in the form:

$$\phi_T = -a\,\phi_{YY} - b\,\phi_{YYYY} + \frac{1}{2}b\,\partial_{YY}\phi^2. \tag{4.5}$$

Introducing the scalings of Y and T:

$$X = \sqrt{\frac{a}{2b}}Y \Leftrightarrow \partial_Y = \sqrt{\frac{a}{2b}}\partial_X, \quad \tau = \frac{a^2}{2b}T \Leftrightarrow \partial_T = \frac{a^2}{2b}\partial_\tau \tag{4.6}$$

eliminates one parameter from equation (4.5) and results in equation that has the form of equation (9) in reference [23]:

$$\phi_\tau = -\phi_{XX} - \frac{1}{2}\phi_{XXXX} + c\,\partial_{XX}\phi^2, \quad c = \frac{b}{2a}. \tag{4.7}$$

LSA of equation (4.7) about the base state $\phi = 1$ gives the perturbation growth rate $\sigma = (1-2c)k^2 - \frac{k^4}{2}$. Thus this base state is longwave unstable at $0 < c < 1/2 \Leftrightarrow 0 < b/a < 1$, with the instability cut-off wavenumber $k_c = \sqrt{2(1-2c)}$. For the computation and estimates I'll use $b = 1, a = 2$, which gives $c = 1/4$ and $k_c = 1$.

Notice that setting $\phi = w_{XX}, c = 1$ in equation (4.7) and integrating twice with respect to X gives $w_\tau = -w_{XX} - w_{XXXX} + w_{XX}^2$ [34]. This equation was rigorously studied in reference [35] (see Eq. (1D MKS) on p. 377 of that paper, which reads $w_\tau = -w_{XX} - w_{XXXX} + (1-\lambda)w_X^2 + \sigma\lambda w_{XX}^2$, with $\lambda = \sigma = 1$). For the 1D MKS equation on a periodic domain these authors proved that depending on the stability of the trivial solution, either: (i) if it is unstable, there exist arbitrarily small initial perturbations that lead to a solution blow-up in a finite time, or (ii) if it is stable, there exist finite-amplitude initial perturbations that lead to a finite-time blow-up. These singularities exhibit self-similar structure in w_{XX}. Their numerical results indicated that w generically becomes pointwise infinite at a finite time. Notice that the limit $\lambda \to 0$ recovers the Kuramoto–Sivashinsky equation which does not exhibit blow-up in one dimension. Also, equation (4.7) with the -1 coefficient of ϕ_{XXXX} and $c = -1$ has been studied in reference [36]. For that equation (the Sivashinsky equation) these authors found an infinite family of self-similar blow-up solutions, performed their LSA, and identified a unique stable blow-up solution. I will refer to equation (4.7) also as Sivashinsky equation.

4.2. Scaling analysis and results

A convenient scaling analysis of a solution singularity development for equation (4.7) was performed in reference [23]. For the sake of clarity I repeat the major points of this analysis in the next paragraph, using my notation.

Let the singularity forms at location $X = 0$ at time $\tau = \tau_s$. For $|X| \ll 1$ and $\tau \lesssim \tau_s$, the variable ϕ varies rapidly with position and ϕ_{XX} is negligible compared to ϕ_{XXXX}. Therefore when seeking the behavior of ϕ close to the singularity, one may consider equation (4.7) without the term $-\phi_{XX}$. Next, rescaling the distance $\tilde{X} = cX$ and time $\tilde{\tau} = c^4\tau$ gives

$$\phi_{\tilde{\tau}} = -\frac{1}{2}\phi_{\tilde{X}\tilde{X}\tilde{X}\tilde{X}} + \frac{1}{c}\partial_{\tilde{X}\tilde{X}}\phi^2. \tag{4.8}$$

One seeks similarity solutions to this equation that have the form

$$\phi(\tilde{\tau}, \tilde{X}) = \frac{1}{c\,(\tilde{\tau}_s - \tilde{\tau})^{\gamma_1}} f\left(\frac{\tilde{X} - \bar{X}}{(\tilde{\tau}_s - \tilde{\tau})^{\gamma_2}}\right), \tag{4.9}$$

where $\bar{X} = \bar{X}(\tilde{\tau})$ is the rescaled position of developing singularity, $\tilde{\tau}_s = c^4\tau_s$ is the rescaled time of singularity formation, $\tilde{\tau} < \tilde{\tau}_s$ and γ_1 and γ_2 are constant exponents. Substitution of equation (4.9) in equation (4.8) yields

$$\phi(\tau, X) = \frac{1}{c\,(\tau_s - \tau)^{1/2}} f(\eta), \tag{4.10}$$

where $\eta = (X - x(\tau))/(\tau_s - \tau)^{1/4}$ is the similarity variable and $x(\tau) = \bar{X}(\tilde{\tau})/c$. Equation (4.10) signals that a downward spike in ϕ develops that is centered at the point $x(\tau)$; the depth of the spike increases as $(\tau_s - \tau)^{-1/2}$ and its width decreases as $(\tau_s - \tau)^{1/4}$ as $\tau \to \tau_s$ from below. The unscaled position of the spike's center moves with velocity $x_\tau \sim (\tau_s - \tau)^{-3/4}$.

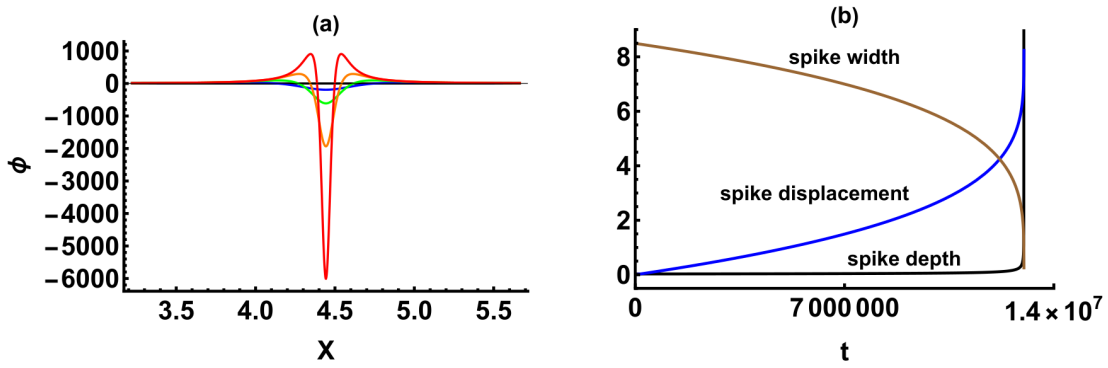

FIGURE 5. (a) Spike formation via computation of equation (4.7) with $c = 1/4$. The initial condition is a small Gaussian-shaped perturbation of the base state $\phi = 1$ on the interval $0 \le X \le 2\sqrt{2}\pi$, where $2\sqrt{2}\pi$ is the most dangerous instability wavelength (the one at which the growth rate ω is the maximum value). Boundary conditions are periodic. The last shown profile corresponds to $\tau_s = 43.35$. Computation was done on a fixed grid in X using 3000 grid points, a fourth-order finite difference discretization formulas in X and a backward difference formulas of variable order in τ. (b) Evolution of the spike dimensions (Eqs. (4.11)–(4.13)) at $\Delta E = 0.01, a = 2, b = 1, t_s = 1.3 \times 10^7$. Proportionality constants $c_{1,2,3} = 1$ are chosen to facilitate plotting three functions on the same plot.

In terms of the original variables used in equation (4.1):

$$\text{spike depth} = \frac{c_1}{\Delta E \sqrt{b\,(t_s - t)}}, \tag{4.11}$$

$$\text{spike width} = c_2 \sqrt{a \Delta E} \left(\frac{t_s - t}{b} \right)^{1/4}, \tag{4.12}$$

$$\text{spike center displacement from } y = 0 = \frac{c_3 \sqrt{a \Delta E}}{b^{1/4}} \left[t_s^{1/4} - (t_s - t)^{1/4} \right], \tag{4.13}$$

where $\Delta E = E - E_c$ and the time of a singularity formation t_s and the proportionality constants $c_{1,2,3}$ can't be determined from the scaling analysis. Obviously, one expects that $t_s = t_s(\Delta E)$, thus equations (4.11)–(4.13) show the dependence of the spike parameters on time, but not yet on ΔE. In order to determine that dependence, first, I use equations (4.2), (4.6), $\epsilon = \Delta E / E_1$, and $a = E_1/4$ to find t_s:

$$t_s = \frac{2 b \tau_s}{a^2 \epsilon^2} = \frac{32 b \tau_s}{\Delta E^2}. \tag{4.14}$$

Next, I compute equation (4.7), see Figure 5a, which gives $\tau_s \approx 40$. Using this value, $b = 1$ and $\Delta E = 0.01$ gives $t_s \approx 1.3 \times 10^7$. Evolution of the spike dimensions at these (fixed) values of ΔE and t_s is shown in Figure 5b. It is seen that in comparison to the singularity of the width and the displacement, the singularity of the depth develops abruptly.

Next, inserting equation (4.14) in equations (4.11)–(4.13) gives the following forms for the dependence of the spike parameters on ΔE and t:

$$\text{spike depth} = \frac{c_1}{b F(t, \Delta E)^2}, \tag{4.15}$$

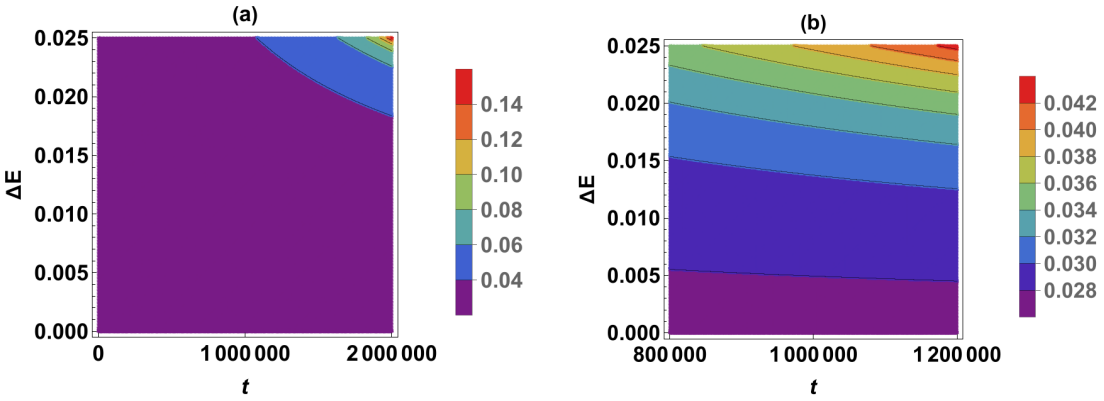

FIGURE 6. Spike depth, as given by equation (4.15). $b = 1, \tau_s = 40, c_1 = 1$. (b) is the zoom view of (a) in the middle of the time interval.

$$\text{spike width} = c_2\sqrt{a}F(t, \Delta E), \tag{4.16}$$

$$\text{spike center displacement from } y = 0 = c_3\sqrt{a}\left[2\left(2\tau_s\right)^{1/4} - F(t, \Delta E)\right], \tag{4.17}$$

where

$$F(t, \Delta E) = \left(32\tau_s - \frac{\Delta E^2 t}{b}\right)^{1/4}. \tag{4.18}$$

Figure 6 shows the major spike dimension, its depth, as the contour plot of the two-variable function (4.15). Spike depth increases as the time and ΔE increase. Moreover, unless the time is close to a blow-up and ΔE is not very small, the depth is more sensitive to ΔE change than to t change. This is the signature of equation (4.18), where the exponent of t is one, and the exponent of ΔE is two. Same is true for the spike width and displacement. Also it is useful to expand equation (4.15) for small ΔE and t:

$$\text{spike depth} = \frac{c_1}{4b\sqrt{2\tau_s}} + \frac{c_1}{256\sqrt{2}b^2\tau_s^{3/2}}\Delta E^2 t + O\left(\Delta E^4 t^2\right). \tag{4.19}$$

This shows that the spike depth grows quadratically in ΔE and only linear in t.

4.3. Steady-state blow-up profile of ϕ

It is interesting to attempt finding a constant (steady-state) solution of equation (4.7) or equation (4.8). In the case of equation (4.7), setting $\phi_\tau = 0$ and integrating twice in X gives:

$$\phi_{XX} + 2\phi - 2c\phi^2 = k_1 X + k_2, \tag{4.20}$$

where k_1, k_2 are the constants of integration. equation (4.20) is the equation of a forced nonlinear oscillator, where X is the "time". I did not succeed in finding a solution of equation (4.20) that would be symmetric, $\phi(-X) = \phi(X)$ and singular at $X = 0$. In the case of equation (4.8), one obtains a steady-state equation

$$\phi_{\tilde{X}\tilde{X}} - \frac{2}{c}\phi^2 = k_1\tilde{X} + k_2. \tag{4.21}$$

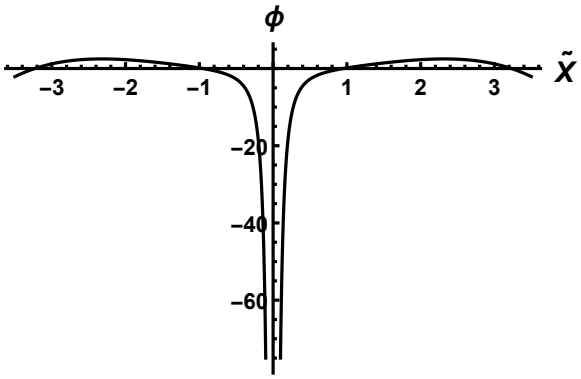

FIGURE 7. Plot of equation (4.22).

At $k_1 = 0$ and arbitrary $c > 0$, Mathematica® finds the general solution of equation (4.21) in terms of Weierstrass elliptic function $W(\tilde{X}, c, k_2, l_1, l_2)$, where l_1, l_2 are arbitrary constants. Remembering that Eqs. (4.8) and (4.21) hold in the vicinity of a spike tip at $\tilde{X} = 0$, a particular symmetric solution that blows up at $\tilde{X} = 0$ and is zero at some distance away from $\tilde{X} = 0$ can be guessed by taking $l_1 = 0$ and some positive values for k_2 and l_2. A power series expansion about $\tilde{X} = 0$ with just a handful of terms very accurately approximates such solution in the vicinity of $\tilde{X} = 0$. For instance, at $k_2 = 10, c = 1/4, l_2 = 2$:

$$\phi = \frac{-3}{4}\tilde{X}^{-2} + \tilde{X}^2 - \frac{2}{21}\tilde{X}^4 + \mathcal{O}\left(\tilde{X}^6\right). \tag{4.22}$$

This is plotted in Figure 7.

Instead of finding a steady-state amplitude spike by the direct integration of the amplitude equation, Bernoff & Bertozzi [35] computed a self-similar blow-up profile for $f(\eta)$, see equation (4.10). Substitute equation (4.10) in equation (4.8), transform to a singular (at $\eta = 0$) third-order equation [35], drop the time derivative, and require the symmetry $f(-\eta) = f(\eta)$. This yields:

$$\frac{1}{2}\eta f_{\eta\eta\eta} - f_{\eta\eta} - \eta\left(f^2\right)_\eta + \frac{1}{4}\eta^2 f + f^2 = f^2(0) - f_{\eta\eta}(0), \tag{4.23}$$

$$f(-\infty) = f(\infty) = f_\eta(0) = 0. \tag{4.24}$$

Bernoff & Bertozzi computed the solution of the above boundary value problem using a shooting method, except the coefficient of $\eta f_{\eta\eta\eta}$ in their equation is equal to one. That solution is shown in Figure 4 of their paper. The shape is visually very similar to the spike in Figure 5a, where the axes are η and f and the profile is shifted to the left, so that the symmetry axis is $\eta = 0$. The smooth minimum of the profile is at $(\eta, f) = (0, -2.169)$ and $f_{\eta\eta}(0) = 2.694$ [35]. Having a coefficient $1/2$ of $\eta f_{\eta\eta\eta}$ in equation (4.23) of course would not change that shape in any significant way.

4.4. Physical estimates

For a gold wire, using $R_0 = 25$ nm, $T = 800°\mathrm{C}$, $D = 5 \times 10^{-7}$ cm^2/s, $\gamma = 1500$ erg/cm^2, $\Omega = 10^{-22}$ cm^3, $\nu = 5 \times 10^{14}$ cm^{-2}, equation (4.14) gives $t_s = 5$ hr. At that temperature, this is the typical physical time of a singularity formation just above the instability threshold ($\Delta E = 0.01$). For comparison, at $T = 600°\mathrm{C}$ this time increases to 50 hr. due to the 10-fold decrease of the diffusivity, and at $T = 800°\mathrm{C}$ and $\Delta E = 0.1$, *i.e.* at the limit of a validity of a weakly nonlinear theory, this time decreases to 3 min. In any case, the pinch-off time predicted by equation (4.14) is significantly larger than the one in experiment; for example, Table 1 in reference [37] suggests that a silver nanowire of 25 nm radius would pinch-off in about 10 min at $T = 300°\mathrm{C}$.

This difference may be the sign that an advanced model that includes a wire heating due to a current crowding is warranted. On the other hand, it should be remembered that the amplitude equation (4.7) is derived assuming a tiny supercriticality ΔE, *i.e.* the system is just above the instability threshold (formally, it is at a distance $\epsilon \ll 1$ above a threshold at all times), thus the amplitude is expected to grow very slow. A weakly nonlinear analysis of any advanced model would have the same limitation on the distance from the instability threshold simply due to a nature of such analysis. Next, one may try to estimate the separation between two parts of a wire upon a pinchoff. In Figure 5a, the width of the spike at the half minimum $\phi \approx -3000$, corresponding to $r \approx 1/2$, is $\Delta X \approx 0.1$. A computation that uses an adaptive mesh refinement at the tip of the spike would be able to follow the spike deepening somewhat longer, thus the half minimum level would shift downward and one may take, say, $\Delta X \approx 0.025$. Then our scalings imply the separation at $r \approx 1/2$, $\Delta y \approx R_0\sqrt{\frac{10}{\Delta E}}\Delta X = 18$ nm at $\Delta E = 0.01, R_0 = 25$ nm, or around 63 atomic diameters of the gold atom. Δy reduces to 6 nm at $\Delta E = 0.1$.

5. A weakly nonlinear multi-scale analysis of the primary modes of instability

5.1. Multiple scales expansion

As was already noted in Introduction, due to the nonlinearity of a governing PDE (2.1) very shortly after the initiation of a morphological instability the initial sinusoidal, single-harmonic form of a solution (the initial condition) ceases to exist, and the solution is represented by a Fourier series. Without loss of generality, I will account only for a handful of major terms in that series, *i.e.* the sinusoidal terms having a wavenumbers that are a small integer multiples of a wavenumber of the primary mode (the sinusoidal initial condition/perturbation) [18], and derive their time-dependent amplitudes. The primary mode has a finite wavenumber $0 < k < k_c$.

I start with the following ansatz for the perturbation of the base state $r = 1$:

$$\begin{aligned} r = 1 &+ \epsilon r_1\left(t_0, t_1, t_2; E\right)\cos ky + \epsilon r_4\left(t_0, t_1, t_2; E\right)\sin ky + \epsilon^2 r_2\left(t_0, t_1, t_2; E\right)\cos 2ky \\ &+\epsilon^2 r_3\left(t_0, t_1, t_2; E\right)\sin 2ky,\ \epsilon \ll 1 \end{aligned} \tag{5.1}$$

where t_0 is the fast time and t_1, t_2 are the slow times. Thus the time derivative reads:

$$\frac{\partial}{\partial t} = \frac{\partial}{\partial t_0} + \epsilon\frac{\partial}{\partial t_1} + \epsilon^2\frac{\partial}{\partial t_2}. \tag{5.2}$$

The initial conditions are chosen as:

$$r_1\left(0, t_1, t_2; E\right) = \xi_0,\ 0 < \xi_0 < 1; \quad r_{2,3,4}\left(0, t_1, t_2; E\right) = 0. \tag{5.3}$$

Now I proceed according to this plan: substitute the expansions (5.1) and (5.2) in equation (2.1), collect the terms of the same powers of ϵ on each of the two sides of the equation and equate them; next, for each of the resulting statements, collect the terms proportional to $\cos ky$, $\sin ky$, $\cos 2ky$, and $\sin 2ky$ on each of the two sides of a statement and equate, separately, the coefficients of these harmonics.

At the order ϵ I get:

$$\frac{\partial r_1}{\partial t_0}\cos ky + \frac{\partial r_4}{\partial t_0}\sin ky = \sigma(k; E) r_1 \cos ky + \sigma(k; E) r_4 \sin ky, \tag{5.4}$$

thus

$$\frac{\partial r_{1,4}}{\partial t_0} = \sigma(k; E) r_{1,4}, \tag{5.5}$$

where the growth rate $\sigma(k; E)$ is given by equation (3.1).

At the order ϵ^2 I get:

$$\frac{\partial r_1}{\partial t_1}\cos ky + \frac{\partial r_4}{\partial t_1}\sin ky + \frac{\partial r_2}{\partial t_0}\cos 2ky + \frac{\partial r_3}{\partial t_0}\sin 2ky = f_1\left(k, r_1, r_4; E\right) + f_2\left(k, r_1, r_4, r_2; E\right)\cos 2ky \\ + f_3\left(k, r_1, r_4, r_3; E\right)\sin 2ky, \tag{5.6}$$

where $f_{1,2,3}$ are certain complicated functions.

5.2. Solutions for r_1 and r_4

$$\frac{\partial r_{1,4}}{\partial t_1} = 0 \rightarrow r_{1,4} = r_{1,4}\left(t_0, t_2; E\right). \tag{5.7}$$

Applying the initial conditions (5.3) and accounting for equation (5.7) I get from the linear ODE (5.5):

$$r_1 = r_1\left(t_0; E\right) = \xi_0 \mathrm{e}^{\sigma(k;E)t_0}, \quad r_4 = 0. \tag{5.8}$$

Here $\sigma(k;E) > 0$, since the case of unstable primary mode is of interest. It can be observed now that the LSA result of Section 3 for the primary mode has been obtained at the linear stage (at order ϵ) of a multi-scale expansion.

5.3. Solutions for r_2 and r_3

Substituting $r_4 = 0$ in f_2 and f_3, for r_2 and r_3 from equation (5.6) one obtains the linear ODEs:

$$\frac{\partial r_{2,3}}{\partial t_0} = f_{2,3}\left(k, r_1, r_{2,3}; E\right) = p(k;E)r_{2,3} + q_{2,3}(k;E)r_1\left(t_0;E\right)^2, \tag{5.9}$$

where

$$p(k;E) = 2\frac{2 + S(1+\cos 2\psi)}{1+S}k^2\left(1-4k^2\right) + 4E\frac{S\sin 2\psi}{1+S}k^2 = \sigma(2k;E), \tag{5.10}$$

$$q_2(k;E) = -3\frac{2 + S(1+\cos 2\psi)}{4(1+S)}k^2\left(1+k^2\right) - E\frac{S\sin 2\psi}{2(1+S)}k^2, \tag{5.11}$$

$$q_3(k;E) = \frac{S\sin 2\psi}{1+S}k^3\left(1-k^2\right) + E\frac{S^2(\cos 4\psi - 1) - S(6\cos 2\psi + 10) - 12}{4(1+S)}k^3. \tag{5.12}$$

Substituting $r_1\left(t_0;E\right)$ from equation (5.8) and taking into account the initial conditions, the solutions of equation (5.9) read:

$$r_{2,3} = r_{2,3}\left(t_0;E\right) = \frac{q_{2,3}(k;E)\xi_0^2}{\sigma(2k;E) - 2\sigma(k;E)}\left[\exp\left(\sigma(2k;E)t_0\right) - \exp\left(2\sigma(k;E)t_0\right)\right]. \tag{5.13}$$

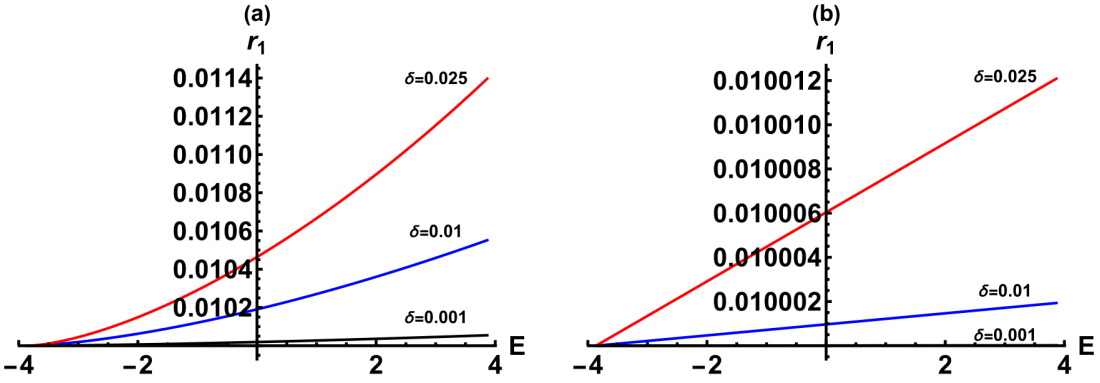

FIGURE 8. The amplitude of $\cos ky$ term in the ansatz (5.1), given by equation (5.8), at $t_0 = 1$, $\xi_0 = 0.01$ for $E_c + 0.01 \le E \le -E_c$, where $E_c = -3.866$. (a) Near the short-wave instability cut-off; (b) Near the long-wave instability threshold.

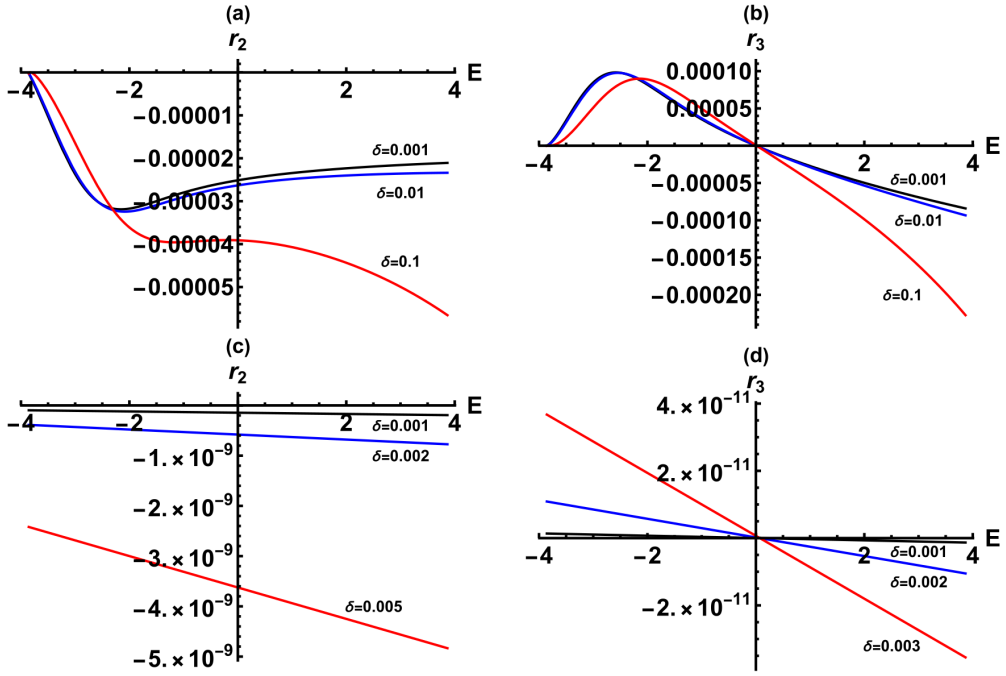

FIGURE 9. The amplitudes of $\cos 2ky$ and $\sin 2ky$ terms in the ansatz (5.1), given by equation (5.13), at $t_0 = 1$, $\xi_0 = 0.01$ for $E_c + 0.01 \le E \le -E_c$, where $E_c = -3.866$. (a, b) Near the short-wave instability cut-off; (c, d) Near the long-wave instability threshold.

5.4. Compatibility condition

Finally, for consistency of equation (5.6) one needs $f_1(k, r_1; E) = 0$. This gives the constraint $k^2\left(k^2 - k_c^2\right) r_1(t_0; E)^2 = 0$, where k_c is seen in equation (3.2). Since $r_1(t_0; E) \neq 0$, either $k = 0$, or $k = k_c$. I proceed below under assumption that the constraint holds approximately at $k = \delta_1$ and $k = k_c - \delta_2$, where

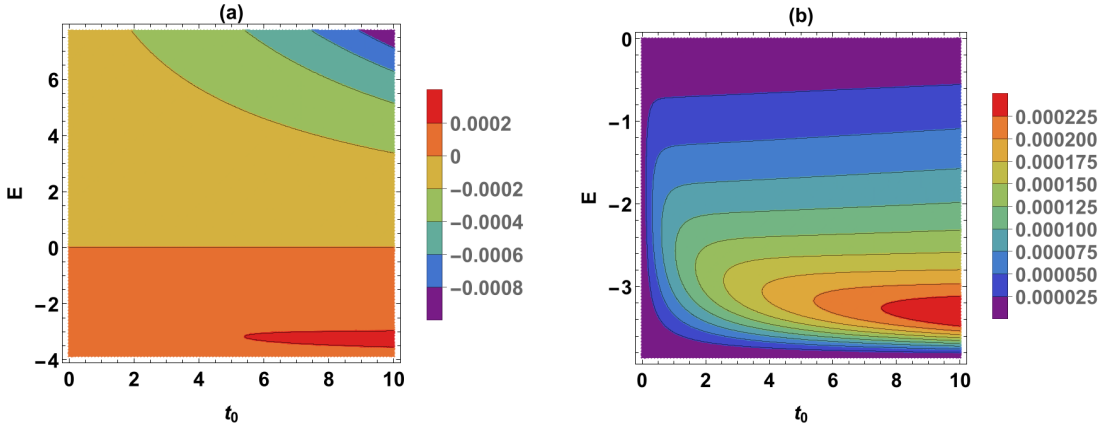

FIGURE 10. The amplitude of $\sin 2ky$ term in the ansatz (5.1), given by equation (5.13), at $\xi_0 = 0.01$, near the short-wave instability cut-off. (b) is the zoom view of the bottom region in (a).

$\delta_{1,2}$ are a positive constants that quantify the deviation from these values into the instability interval $0 < k < k_c$. In particular, $k = \delta_1$ is the most dangerous wavenumber in LSA when $\delta_1 = k_c/\sqrt{2}$.

5.5. Results

Figure 8 shows r_1 as a function of the electric field at fixed t_0 and at various distances δ from the longwave instability threshold $k = 0$ and from the short-wave instability cut-off $k = k_c$. For this, I took $\delta_1 = \delta_2 = \delta$ and substituted $k = \delta$ and $k = k_c - \delta$ in equation (5.8), where $\sigma(k; E)$ and $k_c(E)$ are given by equations (3.1), (3.2). In the former case (Fig. 8b) one can see that $r_1 \sim c_1 \exp(c_2 E), c_1, c_2 = const.$, and values of these constants can be easily calculated. However, for the particular numerical values of the parameters and for the plotting interval these exponential curves are well approximated by the straight lines. In the latter case (Fig. 8a) the analytical dependence on E is complicated, but the curve data can be fitted: $\delta = 0.001$: $r_1 = 0.00997 + 0.000048 \exp(0.145717E)$; $\delta = 0.01$: $r_1 = 0.00973 + 0.000458 \exp(0.153945E)$; $\delta = 0.025$: $r_1 = 0.00941 + 0.001056 \exp(0.16734E)$.

A close look at $r_2(E)$ and $r_3(E)$ curves (Fig. 9) and the comparison to $r_1(E)$ in Figure 8 shows, first, that r_1 is several orders of magnitude larger than $r_{2,3}$. Thus the primary mode $\cos ky$ is dominant in the spectrum, as expected [18]. Next, the absolute values of r_2 are two orders of magnitude larger than the absolute values of r_3 near the longwave instability threshold, while the converse is true near the short-wave instability cut-off. Therefore $\cos 2ky$ and $\sin 2ky$ are the next two fast growing modes in the spectrum.

The largest of $r_{2,3}$ amplitudes, r_3, is plotted in Figure 10 *vs.* t_0 and E near the short-wave instability cut-off. Cross-secting Figure 10a by a vertical cut shows that at any fixed t_0 the amplitude dependence on E is roughly as seen in Figure 9b. Moreover, a (positive) maximum of the amplitude increases with t_0, as seen in Figure 10b.

6. SUMMARY

Provided that the electric field slightly exceeds a threshold value that is necessary for initiation of a morphological instability, the weakly nonlinear analysis that I carried out shows for the first time the electric field-and-time dependence of the dimensions of the focusing self-similar perturbation's amplitude profile approaching a blow-up. That amplitude singularity marks a wire pinch-off and its breakup into a chain of nanoparticles. In particular, this analysis shows that the amplitude initially grows quadratically in the deviation from a threshold value of the electric field. For the initial surface perturbation of the form $\xi_0 \cos ky$, $0 < \xi_0 < 1$ (where y is the axial

variable) a separate, multi-scale analysis of a weakly nonlinear phase of the instability shows that in that regime the fastest growing instability modes are $\cos ky$, $\cos 2ky$, and $\sin 2ky$, and for these modes I found the explicit dependence of their amplitudes on time and the strength of the applied electric field.

Acknowledgements

The author thanks Alexander A. Nepomnyashchy and Mark R. Bradley for very useful suggestions and discussions regarding the analysis in Section 4. Mark R. Bradley is also acknowledged for bringing his paper [23] to author's attention and for pointing to reference [35].

References

[1] H.B. Huntington, Electromigration in metals, in: Diffusion in Solids: Recent Developments, edited by A.S. Nowick. Academic Press (1975) Ch. 6.
[2] P.S. Ho and T. Kwok, Electromigration in metals. *Rep. Prog. Phys.* **52** (1989) 301–348.
[3] P.J. Rous, T.L. Einstein and E.D. Williams, Theory of surface electromigration on metals: application to self-electromigration on Cu(111). *Surf. Sci.* **315** (1994) L995–L1002.
[4] H. Park, A.K.L. Lim, A. Paul Alivisatos, J. Park and Paul L. McEuen, Fabrication of metallic electrodes with nanometer separation by electromigration. *Appl. Phys. Lett.* **75** (1999) 301.
[5] L. Valladares, L.L. Felix, A.B. Dominguez, T. Mitrelias, F. Sfigakis, S.I. Khondaker, C.H.W. Barnes and Y. Majima, Controlled electroplating and electromigration in nickel electrodes for nanogap formation. *Nanotechnology* **21** (2010) 445304.
[6] L. Arzubiaga, F. Golmar, R. Liopis, F. Casanova and L.E. Hueso, Tailoring palladium nanocontacts by electromigration. *Appl. Phys. Lett.* **102** (2013) 193103.
[7] R. Hoffmann-Vogel, Electromigration and the structure of metallic nanocontacts. *Appl. Phys. Rev.* **4** (2017) 031302.
[8] F.A. Nichols and W.W. Mullins, Surface-(interface-) and volume-diffusion contributions to morphological changes driven by capillarity. *Trans. Metall. Soc. AIME* **233** (1965) 1840–1848.
[9] F.A. Nichols and W.W. Mullins, Morphological changes of a surface of revolution due to capillarity induced surface diffusion. *J. Appl. Phys.* **36** (1965) 1826.
[10] J.W. Cahn, Stability of rods with anisotropic surface free energy. *Scripta Metall.* **13** (1979) 1069–1071.
[11] A.J. Bernoff, A.L. Bertozzi and T.P. Witelski, Axisymmetric surface diffusion: dynamics and stability of self-similar pinchoff. *J. Stat. Phys.* **93** (1998) 725–776.
[12] B.D. Coleman, R.S. Falk and M. Moakher, Stability of cylindrical bodies in the theory of surface diffusion. *Physica D* **89** (1995) 123–135.
[13] M.S. McCallum, P.W. Voorhees, M.J. Miksis, S.H. Davis, and H. Wong, Capillary instabilities in solid thin films: lines. *J. Appl. Phys.* **79** (1996) 7604.
[14] H. Wong, M.J. Miksis, P.W. Voorhees and S.H. Davis, Universal pinch off of rods by capillarity-driven surface diffusion. *Scripta Mater.* **39** (1998) 55–60.
[15] D.J. Kirill, S.H. Davis, M.J. Miksis and P.W. Voorhees, Morphological instability of a whisker. *Proc. R. Soc. Lond. A* **455** (1999) 3825–3844.
[16] K.F. Gurski and G.B. McFadden, The effect of anisotropic surface energy on the Rayleigh instability. *Proc. R. Soc. Lond. A* **459** (2003) 2575–2598.
[17] K.F. Gurski, G.B. McFadden and M.J. Miksis, The effect of contact lines on the Rayleigh instability with anisotropic surface energy. *SIAM J. Appl. Math.* **66** (2006) 1163–1187.
[18] F. Wang, O. Tschukin, T. Leisner, H. Zhang, B. Nestler, M. Selzer, G.C. Marques and J. Aghassi-Hagmann, Morphological stability of rod-shaped continuous phases. *Acta Materialia* **192** (2020) 20–29.
[19] V. Gorshkov and V. Pivman, Kinetic Monte Carlo model of breakup of nanowires into chains of nanoparticles. *J. Appl. Phys.* **122** (2017) 204301.
[20] M. Khenner, Effect of electromigration on onset of morphological instability of a nanowire. *J. Eng. Math.* **140** (2023) 6.
[21] M. Khenner, Nanowire breakup via a morphological instability enhanced by surface electromigration. *Model. Simul. Mater. Sci. Eng.* **32** (2024) 015003.

[22] T.F. Marinis, R.F. Sekerka, F.D. Lemkey, H.E. Cline and M. McLean, In-Situ Composites IV. Elsevier, NY (1982) 315–327.
[23] M.P. Gelfand and R.M. Bradley, One dimensional conservative surface dynamics with broken parity: Arrested collapse versus coarsening. *Phys. Lett. A* **379** (2015) 199–205.
[24] S. Xu, P.F. Li and Y. Lu, In situ atomic-scale analysis of Rayleigh instability in ultrathin gold nanowires. *Nano Res.* **11** (2018) 625.
[25] S. Karim, M.E. Toimil-Molares, A.G. Balogh, W. Ensinger, T.W. Cornelius, E.U. Khan and R. Neumann, Morphological evolution of Au nanowires controlled by Rayleigh instability. *Nanotechnology* **17** (2006) 5954–5959.
[26] M. Schimschak and J. Krug, Surface electromigration as a moving boundary value problem. *Phys. Rev. Lett.* **78** (1997) 278.
[27] L. Du and D. Maroudas, Optimization of electrical treatment strategy for surface roughness reduction in conducting thin films. *J. Appl. Phys.* **124** (2018) 125302.
[28] R.M. Bradley, Electromigration-induced shock waves on metal thin films. *Appl. Phys. Lett.* **93** (2008) 213105.
[29] R.M. Bradley, Shock waves on current-carrying metal thin films. *Phys. Rev. B* **79** (2009) 075403.
[30] M. Yagi and J. Shirakashi, Evolution of local temperature in Au nanowires during feedback-controlled electromigration observed by atomic force microscopy. *Appl. Phys. Lett.* **110** (2017) 203105.
[31] R.S. Timsit, Remarks on the thermal stability of an Ohmic-heated nanowire. *J. Appl. Phys.* **123** (2018) 175105.
[32] H. Suga, H. Suzuki, K. Otsu, T. Abe, Y. Umeta, K. Tsukagoshi, T. Sumiya, H. Shima, H. Akinaga and Y. Naitoh, Feedback electromigration assisted by alternative voltage operation for the fabrication of facet-edge nanogap electrodes. *ACS Appl. Nano Mater.* **3** (2020) 4077–4083.
[33] S. Karim, M.E. Toimil-Molares, W. Ensinger, A.G. Balogh, T.W. Cornelius, E.U Khan and R. Neumann, Influence of crystallinity on the Rayleigh instability of gold nanowires. *J. Phys. D: Appl. Phys.* **400** (2007) 3767–3770.
[34] R.M. Bradley, private communication.
[35] A.J. Bernoff and A.L. Bertozzi, Singularities in a modified Kuramoto–Sivashinsky equation describing interface motion for phase transition. *Physica D* **85** (1995) 375–404.
[36] A.J. Bernoff and T.P. Witelski, Stability and dynamics of self-similarity in evolution equations. *J. Eng. Math.* **66** (2010) 11–31.
[37] F. Balty, A. Baret, A. Silhanek and N.D. Nguyen, Insight into the morphological instability of metallic nanowires under thermal stress. *J. Colloid Int. Sci.* **673** (2024) 574–582.